arXiv:astro-ph/0407604v1 29 Jul 2004

Quintessence and the Transition to an Accelerating Universe

Carl L. Gardner
gardner@math.asu.edu
Department of Mathematics and Statistics
Arizona State University
Tempe AZ 85287-1804

Abstract

The implications of seven popular models of quintessence based on supergravity or M/string theory for the transition from a decelerating to an accelerating universe are explored.

All seven potentials can mimic the ΛCDM model at low redshifts $0 \leq z \leq 5$. However, for a natural range of initial values of the quintessence field, the SUGRA and Polónyi potentials predict a transition redshift $z_t \approx 0.5$ for $\Omega_{\Lambda 0} = 0.70$, in agreement with the observational value $z_t \approx 0.46$ and in mild conflict with the ΛCDM value $z_t = 0.67$.

Tables are given for the quintessence potentials for the recent average $\overline{w}_0$ of the equation of state parameter, and for w_0 and w_1 in the low-z approximation $w \approx w_0 + w_1 z$.

It is argued that for the exponential potential $e^{\lambda\varphi}$ to produce a viable present-day cosmology, $\lambda \leq \sqrt{2}$.

A robust, scaled numerical method is presented for simulating the cosmological evolution of the scalar field.

1 Introduction

In the standard ΛCDM cosmological model, the universe makes a transition from deceleration to acceleration at a redshift $z_t = 0.67$ for $\Omega_{\Lambda 0} = 0.70$.

This prediction is to be contrasted with the observational value $z_t = 0.46 \pm 0.13$ from the distance-redshift diagram for type Ia supernovae (SNe Ia) [1]. With further observations, the SNe Ia data may converge to the ΛCDM value. However the value $z_t \approx 0.46$ could be a signal of the effects of a quintessence scalar field, extra spatial dimensions, and/or modifications to general relativity.

For the spatially homogeneous quintessence scalar field ϕ, define the equation of state parameter $w = w(z) = P_\phi/\rho_\phi$, where the scalar field pressure P_ϕ and energy density ρ_ϕ are given by

$$P_\phi = \frac{1}{2}\dot{\phi}^2 - V(\phi), \quad \rho_\phi = \frac{1}{2}\dot{\phi}^2 + V(\phi). \tag{1}$$

The SNe Ia observations [1] bound the recent ($z \leq 1.75$) average $\overline{w}_0 < -0.76$ (95% CL) assuming $\overline{w}_0 \geq -1$, and measure $z_t = 0.46 \pm 0.13$. Alternatively, the SNe Ia data place bounds $-1 < w_0 < -0.72$ (95% CL) and $w_1 = 0.6 \pm 0.5$, where $w(z) \approx w_0 + w_1 z$ for $z \lesssim 1$. This investigation will explore seven popular models of quintessence (see Table 1), and compare and contrast their predictions for z_t, $\overline{w}_0$, w_0, and w_1. These models are basically the ones analyzed in Ref. [2] in terms of dark energy and the fate of the universe (see also Refs. [3, 4]).

We will assume a flat Friedmann-Robertson-Walker universe. In the ΛCDM model, the total energy density $\rho = \rho_m + \rho_r + \rho_\Lambda = \rho_c$, where ρ_c is the critical density for a flat universe and ρ_m, ρ_r, and ρ_Λ are the energy densities in (nonrelativistic) matter, radiation, and the cosmological constant respectively. In the quintessence/cold dark matter (QCDM) model, $\rho = \rho_m + \rho_r + \rho_\phi = \rho_c$. Ratios of energy densities to the critical density will be denoted by $\Omega_m = \rho_m/\rho_c$, $\Omega_r = \rho_r/\rho_c$, $\Omega_\Lambda = \rho_\Lambda/\rho_c$, and $\Omega_\phi = \rho_\phi/\rho_c$, while ratios of present energy densities to the present critical density will be denoted by Ω_{m0}, Ω_{r0}, $\Omega_{\Lambda 0}$, and $\Omega_{\phi 0} \equiv \Omega_{\Lambda 0}$.

In the ΛCDM model,

$$z_t = \left(\frac{2\Omega_{\Lambda 0}}{\Omega_{m0}}\right)^{1/3} - 1. \tag{2}$$

From WMAP + SDSS [5], $\Omega_{\Lambda 0} = 0.71^{+0.03}_{-0.05}$. For the 1σ lower bound on $\Omega_{\Lambda 0}$, $z_t = 0.57$, which is just at the upper 1σ bound for the measured z_t. Thus the ΛCDM model value for z_t lies at the boundary of the joint 68% confidence interval of the SNe Ia data. We are here interested, however, in whether

dimensionless V	*name*
$e^{\lambda\varphi}$	exponential
$\cosh(\sqrt{2}\varphi)$	cosh (stable de Sitter)
$2-\cosh(\sqrt{2}\varphi)$	cosh (unstable de Sitter)
$1+\cos(\varphi)$	axion
$\cos(\varphi)$	axion (unstable de Sitter)
$\left[\left(1+\frac{\varphi}{\sqrt{2}}\left(\frac{\varphi}{\sqrt{2}}+\beta\right)\right)^2-3\left(\frac{\varphi}{\sqrt{2}}+\beta\right)^2\right]e^{\varphi^2/2}$	Polónyi
$e^{\varphi^2/2}/\varphi^4$	SUGRA

Table 1: Quintessence potentials inspired by supergravity or M/string theory. $\varphi=\phi/M_P$.

quintessence models satisfying the observational bounds on $\overline{w}_0$ and w_0 may be in better agreement with the measured central value for z_t and consistent with the 1σ limits on w_1. Of the seven models in Table 1, all but two are very close to the ΛCDM model values for z_t and $w_1=0$ (in fact, $z_t\geq 0.67$ for $\Omega_{\phi 0}=0.70$), while the SUGRA and Polónyi potentials differ qualitatively from the others in their predictions for z_t and w_1, and in a certain natural parameter range agree closely with the observed central values.

All seven potentials can mimic the ΛCDM model at low redshifts $0\leq z\leq 5$ to well within the observational error bounds. If the SNe Ia data converge to the ΛCDM value for z_t, then further restrictions can be placed on the possible initial values for ϕ and on parameters in the potentials. For the SUGRA and Polónyi potentials to mimic a cosmological constant at present, the initial values for ϕ must be fine tuned; these models can naturally predict $z_t\approx 0.5$ for $\Omega_{\Lambda 0}=0.70$.

Ref. [6] gave w_0 equal to -0.8 to -0.9 and $w_1\approx 0.3$–0.45 for the SUGRA potential $e^{\varphi^2/2}/\varphi^\alpha$ for $2\leq\alpha\leq 16$—in agreement with our results for $\alpha=4$ for a range of initial values $0<\varphi_i=\phi_i/M_P\lesssim 1$.

Curves for Ω_ϕ and $w(z)$ for the cosh, SUGRA ($\varphi_i=1$ and $\alpha=11$ only), and Polónyi ($\varphi_i=-1$ only) potentials were given in Ref. [2]; where they overlap, our results agree with theirs. The main focus here, however, is on the transition redshift, which was not addressed in Ref. [2].

Mention should also be made of Ref. [7], which investigated the implication of a 5D brane world modification of general relativity [8] for the recent acceleration of the universe and found $z_t\approx 0.5$.

2 Cosmological Equations

The homogeneous scalar field obeys the Klein-Gordon equation

$$\ddot{\phi} + 3H\dot{\phi} = -\frac{dV}{d\phi} \equiv -V_\phi. \tag{3}$$

The Hubble parameter H is related to the scale factor a and the energy densities in matter, radiation, and the quintessence field through the Friedmann equation

$$H^2 = \left(\frac{\dot{a}}{a}\right)^2 = \frac{\rho}{3M_P^2} = \frac{1}{3M_P^2}\left(\frac{1}{2}\dot{\phi}^2 + V(\phi) + \rho_m + \rho_r\right) \tag{4}$$

where the (reduced) Planck mass $M_P = 2.4 \times 10^{18}$ GeV.

We will use the logarithmic time variable $\tau = \ln(a/a_0) = -\ln(1+z)$. Note that for de Sitter space $\tau = H_\Lambda t$, where $H_\Lambda^2 = \rho_\Lambda/(3M_P^2)$, and that $H_\Lambda t$ is a useful time variable for the era of Λ-matter domination (see e.g. Ref. [9]). Also note that for $0 \le z \le z_{BBN} = 10^{10}$, $-23.03 \le \tau \le 0$, where BBN denotes the era of big-bang nucleosynthesis. (BBN occurs over a range of $z \approx 10^9$–10^{10}; we will take $z_{BBN} \equiv 10^{10}$.)

For numerical simulations, the cosmological equations should be put into dimensionless form. Eqs. (3) and (4) can be cast in the form of a system of two first-order equations in τ plus a scaled version of H:

$$\overline{H}\varphi' = \psi \tag{5}$$

$$\overline{H}(\psi' + 3\psi) = -3\overline{V}_\varphi \tag{6}$$

$$\overline{H}^2 = \frac{1}{6}\psi^2 + \overline{V} + \overline{\rho}_m + \overline{\rho}_r \tag{7}$$

where $\overline{H} = H/H_0$, $\varphi = \phi/M_P$, $\overline{V} = V/\rho_{c0}$, $\overline{\rho}_m = \rho_m/\rho_{c0}$, $\overline{\rho}_r = \rho_r/\rho_{c0}$, and a prime denotes differentiation with respect to τ: $\varphi' = d\varphi/d\tau$, etc.

A further scaling may be performed resulting in a set of equations which is numerically more robust, especially before the time of BBN:

$$\tilde{H}\varphi' = \tilde{\psi} \tag{8}$$

$$\tilde{H}(\tilde{\psi}' + \tilde{\psi}) = -3\tilde{V}_\varphi \tag{9}$$

$$\tilde{H}^2 = \frac{1}{6}\tilde{\psi}^2 + \tilde{V} + \tilde{\rho}_m + \tilde{\rho}_r \tag{10}$$

where $\tilde{H} = e^{2\tau}H/H_0$, $\tilde{\psi} = e^{2\tau}\psi$, $\tilde{V} = e^{4\tau}V/\rho_{c0}$, $\tilde{\rho}_m = e^{4\tau}\rho_m/\rho_{c0}$, and $\tilde{\rho}_r = e^{4\tau}\rho_r/\rho_{c0}$.

Figure 1 illustrates (for the exponential potential $e^{\sqrt{2}\varphi}$) that while $\tilde{H}$ varies over only two orders of magnitude between BBN and the present, $\overline{H}$ varies over eighteen orders of magnitude. A similar scaling effect occurs for $\tilde{\psi}$ vs. ψ.

We define the recent average of the equation of state parameter w by rewriting the conservation of energy equation

$$\dot{\rho} + 3H(\rho + P) = 0 \tag{11}$$

where P is the pressure, as

$$0 = \rho' + 3(\rho + P) = \sum_j \rho_j' + 3\sum_j (1 + w_j)\rho_j \tag{12}$$

where $j = m,\, r,\, \phi$. The solution is

$$\rho_j = \rho_{j0} \exp\left\{-3\int_0^\tau (1 + w_j)d\tau\right\}. \tag{13}$$

Note that $w_m = 0$ and $w_r = 1/3$ are constant except near particle-antiparticle thresholds. The recent average of $w_\phi \equiv w$ is defined as

$$\overline{w}_0 = \frac{1}{\tau}\int_0^\tau w d\tau. \tag{14}$$

We will take the upper limit of integration τ to correspond to $z = 1.75$.

Strictly speaking,

$$\rho_m = \rho_{m0}e^{-3\tau}f_m(\tau), \quad \rho_r = \rho_{r0}e^{-4\tau}f_r(\tau) \tag{15}$$

where $f_m(\tau)$ and $f_r(\tau)$ (with $f_m(0) = 1 = f_r(0)$) account for the change in the effective number $\mathcal{N}(T)$ of massless degrees of freedom as τ decreases and the temperature T of the gas of relativistic particles increases. Below $T = 1$ MeV at z_{BBN}, $\mathcal{N} = 3.36$ is constant, so we can safely set $f_m(\tau) = 1$ since $\rho_m \sim (1 + z)^3$ quickly becomes negligible compared to $\rho_r \sim (1 + z)^4$ for $z > z_{m-r} = 3233$ at the equality of matter and radiation densities. In computing the evolution of the quintessence field, we will start with initial conditions at z_{BBN}, so we can also set $f_r(\tau) = 1$ for our purposes. Thus in Eqs. (7) and (10),

$$\overline{\rho}_m + \overline{\rho}_r = \Omega_{m0}e^{-3\tau} + \Omega_{r0}e^{-4\tau} \tag{16}$$

$$\tilde{\rho}_m + \tilde{\rho}_r = \Omega_{m0} e^{\tau} + \Omega_{r0}. \tag{17}$$

(Ref. [10] suggests the phenomenological form $f_r(\tau) = e^{-\tau/15}$ for z going as far back as 10^{30}.)

The transition redshift z_t is defined through the acceleration Friedmann equation

$$\frac{\ddot{a}}{a} = -\frac{1}{6M_P^2}(\rho + 3P) \tag{18}$$

which may be written in the form

$$-q = \frac{1}{H^2}\frac{\ddot{a}}{a} = \frac{H'}{H} = -\frac{1}{2}(\Omega_m + 2\Omega_r + (1+3w)\Omega_\phi) \tag{19}$$

where $-q$ is the acceleration parameter. The Friedmann equation (4), conservation of energy equation (11), and the acceleration equation (18) are related by the Bianchi identities, so that only two are independent. Eq. (11) gives the evolution (15) of ρ_m and ρ_r, and the Klein-Gordon equation (3) for the weakly coupled scalar field. When a cosmological model involves a collapsing stage where H reverses sign, Eq. (18) should be used instead of Eq. (4). In computational form, the acceleration equation becomes

$$\overline{H}\ \overline{H}' = -\frac{1}{2}\overline{\rho}_m - \overline{\rho}_r - \frac{1}{3}\psi^2 + \overline{V} \tag{20}$$

or

$$\tilde{H}\tilde{H}' - 2\tilde{H}^2 = -\frac{1}{2}\tilde{\rho}_m - \tilde{\rho}_r - \frac{1}{3}\tilde{\psi}^2 + \tilde{V}. \tag{21}$$

3 Simulations

For the computations below, we will use Eqs. (8)–(10) with initial conditions specified at z_{BBN} by φ_i and $\dot{\varphi}_i \propto \psi_i = 0$. The potential $V = A\cdot$(dimensionless potential), where the dimensionless potentials are given in Table 1. The constant A is adjusted by a bisection search method so that $\Omega_{\phi 0} = \Omega_{\Lambda 0}$. This involves the usual single fine tuning.

Since several observational lines including SNe Ia, the cosmic microwave background (CMB), large scale structure (LSS) formation, the integrated Sachs-Wolfe effect, and gravitational lensing measure $0.66 \leq \Omega_{\Lambda 0} \leq 0.74$, we will restrict our analysis to this interval, even though technically the bounds are 1σ. Our main line of development will take $\Omega_{\Lambda 0} = 0.70$; in passing, we

will make some remarks about what changes if $\Omega_{\Lambda 0} = 0.66$. The main effect of changing $\Omega_{\Lambda 0}$ to 0.66 (0.74) is to shift the acceleration curves toward the left (right).

We will consider an ultra-light scalar field with $m_\phi^2 \sim H_\Lambda^2$; then ϕ "sits and waits" during the early evolution of the universe, and only starts moving when $H^2 \sim m_\phi^2$. In this way it is easy to satisfy the BBN ($z \sim 10^9$–10^{11}), CMB ($z \sim 10^3$–10^5), and LSS ($z \sim 10$–10^4) bounds on $\Omega_\phi \lesssim 0.1$. An ultra-light scalar field also reflects the observational evidence that the universe has only recently made the transition from deceleration to acceleration and has only recently become dominated by dark energy.

Ultra-light scalar fields exist near de Sitter space extrema in 4D extended gauged supergravity theories (with noncompact internal spaces), with quantized mass squared [11, 12, 3, 13, 14, 15]

$$m^2 = nH_\Lambda^2, \quad H_\Lambda^2 = \frac{\rho_{\Lambda Q}}{3M_P^2} \tag{22}$$

where $-6 \leq n \leq 12$ is an integer. In this context H_Λ is the de Sitter space value of H with effective cosmological constant $\rho_{\Lambda Q}$ at the extremum of the quintessence potential V. Note that to produce the current acceleration of the universe, typically $\rho_{\Lambda Q} \approx \rho_\Lambda$, but does not equal ρ_Λ unless the quintessence field—unlike the ones below—is at a de Sitter extremum at t_0. In certain cases, these theories are directly related to M/string theory. An additional advantage of these theories is that the classical values $m^2 = nH_\Lambda^2$ and $\rho_{\Lambda Q}$ are protected against quantum corrections. The relation $m^2 = nH_\Lambda^2$ was derived for supergravity with scalar fields; in the presence of other matter fields, the relation may be modified.

3.1 Exponential Potential

The exponential potential $e^{\lambda\varphi}$ [16, 17, 18, 19] can be derived from M-theory [20] or from $N = 2$, 4D gauged supergravity [21]. The results for $V = Ae^{\lambda\varphi}$ are independent of the initial value φ_i, which we arbitrarily set equal to 1.

For $\lambda^2 > 3$, the cosmological equations have a global attractor with $\Omega_\phi = n/\lambda^2$, where $n = 3$ for the matter dominated era (during which $w = 0$) or $n = 4$ for the radiation dominated era (during which $w = 1/3$). For $\lambda^2 < 3$, the cosmological equations have a late time attractor with $\Omega_\phi = 1$ and $w = \lambda^2/3 - 1$. In the simulations presented here (see Figs. 2–5 and

λ	$\overline{w}_0$	z_t	w_0	w_1
$1/\sqrt{3}$	-0.98	0.68	-0.95	-0.07
1	-0.93	0.71	-0.84	-0.19
$\sqrt{2}$	-0.83	0.76	-0.68	-0.33
$\sqrt{3}$	-0.70	0.76	-0.49	-0.40
2	-0.50		-0.27	-0.37

Table 2: Parameters for the potential $e^{\lambda\varphi}$.

Table 2), the scalar field is still evolving at t_0 toward the attractor solution, as advocated in Refs. [22, 23, 2].

For $\lambda = \sqrt{2}$ and $\rho_m = 0$, $\ddot{a} \to 0$ asymptotically; if $\rho_m > 0$, the universe eventually enters a future epoch of deceleration. In either case, there is no event horizon. For $\lambda < \sqrt{2}$, the universe enters a period of eternal acceleration with an event horizon. For $\lambda > \sqrt{2}$, the universe eventually decelerates and there is no event horizon.

The ΛCDM cosmology is approached for $\lambda \leq 1/\sqrt{3}$. Significant acceleration occurs only for $\lambda \lesssim \sqrt{3}$. For $\lambda = \sqrt{3}$, w_0 is much too high; setting $\Omega_{\phi 0} = 0.66$ still results in $w_0 = -0.54$. We conclude that $\lambda \leq \sqrt{2}$ in the exponential potential for a viable present-day cosmology.

3.2 Stable de Sitter Cosh Potential

The $\cosh(\sqrt{2}\varphi)$ potential exemplifies $N = 2$ supergravity with a future de Sitter space [14, 15], with $m_\phi^2 = 6H_\Lambda^2$.

φ_i	$\overline{w}_0$	z_t	w_0	w_1
0.1	-0.998	0.67	-0.997	0.001
0.5	-0.96	0.68	-0.94	0.005
1	-0.89	0.72	-0.81	-0.08
2	-0.84	0.75	-0.69	-0.30

Table 3: Parameters for the potential $\cosh(\sqrt{2}\varphi)$.

Results for the cosh potential are presented in Figs. 6–9 and Table 3. Near t_0, φ is evolving toward the minimum of the potential. The ΛCDM model is approached as $\varphi_i \to 0$. For $\varphi_i \geq 2$, the $\cosh(\sqrt{2}\varphi)$ results are very nearly the same as for $e^{\sqrt{2}\varphi}$.

3.3 Unstable de Sitter Cosh Potential

The $2 - \cosh(\sqrt{2}\varphi)$ potential is derived from M-theory/$N = 8$ supergravity [24], with $m_\phi^2 = -6H_\Lambda^2$ at the maximum of the potential. Near the unstable de Sitter maximum ($\varphi_i \to 0$), the universe can mimic ΛCDM for a very long time (on the order of or greater than t_0) [2].

φ_i	$\overline{w}_0$	z_t	w_0	w_1
0.1	-0.996	0.67	-0.99	-0.04
0.2	-0.98	0.69	-0.93	-0.24
0.3	-0.92	0.77	-0.64	-1.8

Table 4: Parameters for the potential $2 - \cosh(\sqrt{2}\varphi)$.

Results for the unstable de Sitter cosh potential are presented in Figs. 10–13 and Table 4. The scalar field is just beginning to grow without bound at t_0. For $\varphi_i \geq 0.33$, $\Omega_{\phi 0}$ never reaches 0.70; for $\varphi_i \geq 0.35$, $\Omega_{\phi 0}$ never reaches 0.66.

3.4 Axion Potential

For the axion potentials $1 + \cos(\lambda\varphi)$ and $\cos(\lambda\varphi)$ in this and the next subsection, we can restrict our attention to $0 \leq \lambda\varphi_i \leq \pi$. We will set $\lambda = 1$; similar results are obtained for $\lambda = \sqrt{2}$.

The axion potential $1 + \cos(\varphi)$ is based on $N = 1$ supergravity [25, 26], with $m_\phi^2 = 3H_\Lambda^2$. As $\varphi \to \pi$, the universe evolves to Minkowski space.

φ_i/π	$\overline{w}_0$	z_t	w_0	w_1
0.1	-0.998	0.67	-0.995	-0.01
0.3	-0.98	0.68	-0.95	-0.10
0.5	-0.90	0.75	-0.74	-0.55
0.55	-0.83	0.82	-0.55	-1.1

Table 5: Parameters for the potential $1 + \cos(\varphi)$.

Figures 14–17 and Table 5 present the results for the axion potential. As $\varphi_i \to 0$, a transient de Sitter universe is obtained that mimics the ΛCDM model for a long time. Near t_0, φ is beginning to evolve toward π. For $\varphi_i/\pi \geq 0.59$, $\Omega_{\phi 0} = 0.70$ is never attained; for $\varphi_i/\pi > 0.61$, $\Omega_{\phi 0}$ never reaches 0.66.

3.5 Unstable de Sitter Axion Potential

The unstable de Sitter axion potential $\cos(\varphi)$ is based on M/string theory reduced to an effective $N = 1$ supergravity theory [27], with $m_\phi^2 = -3H_\Lambda^2$ at the maximum of V.

φ_i/π	$\overline{w}_0$	z_t	w_0	w_1
0.05	-0.998	0.67	-0.99	-0.01
0.10	-0.99	0.68	-0.98	-0.06
0.15	-0.98	0.69	-0.93	-0.16
0.20	-0.94	0.72	-0.83	-0.47
0.25	-0.78	0.94	-0.16	-4.4

Table 6: Parameters for the potential $\cos(\varphi)$.

Results for the unstable axion potential are presented in Figs. 18–21 and Table 6. An unstable de Sitter universe that mimics ΛCDM for a long time [2] is obtained as $\varphi_i \to 0$. Near t_0, φ is beginning to evolve toward π. For $\varphi_i/\pi = 0.25$, there is a transition back to deceleration at $z_t = 0.12$.

3.6 Polónyi Potential

The Polónyi potential $\left[\left(1 + \frac{\varphi}{\sqrt{2}}\left(\frac{\varphi}{\sqrt{2}} + \beta\right)\right)^2 - 3\left(\frac{\varphi}{\sqrt{2}} + \beta\right)^2\right] e^{\varphi^2/2}$ is derived from $N = 1$ supergravity [28] (for a review, see Ref. [29]). The potential is invariant under the transformation $\varphi \to -\varphi$, $\beta \to -\beta$.

Following Ref. [2], we will take $m_\phi^2 \sim \rho_\Lambda/M_P^2$ and set $\beta = 2 - \sqrt{3}$, 0.2, and 0.4, for which the universe asymptotically evolves to Minkowski space, de Sitter space, or a collapse respectively (see Fig. 22). Figures 23–26 and Table 7 have $\beta = 2 - \sqrt{3}$. For this value of β, $\Omega_{\phi 0} = 0.70$ is not reached for $\varphi_i \geq 0.09$. Ω_ϕ begins to violate the LSS bound as φ_i goes below -2.5. The ΛCDM model is approximated for $\varphi_i \approx -0.5$. At t_0, φ is beginning to evolve toward the location $\varphi = \sqrt{2}(\sqrt{3} - 1)$ of the minimum of the potential. For $-2.0 \lesssim \varphi_i \lesssim -1.5$, $z_t \approx 0.5$ and at least w_0 and w_1 satisfy the observational bounds.

Tables 8 and 9 demonstrate that a transition redshift $z_t \approx 0.4$–0.5 is not an accident due to the particular choice $\beta = 2 - \sqrt{3}$.

φ_i	$\overline{w}_0$	z_t	w_0	w_1
0.05	-0.85	0.81	-0.54	-1.7
0	-0.89	0.76	-0.68	-0.96
-0.5	-0.96	0.69	-0.91	-0.13
-1.0	-0.92	0.70	-0.87	-0.07
-1.5	-0.74	0.57	-0.74	0.16
-1.6	-0.69	0.49	-0.73	0.21
-1.7	-0.64	0.43	-0.72	0.26
-1.8	-0.59	0.39	-0.71	0.30
-1.9	-0.56	0.36	-0.71	0.32
-2.0	-0.53	0.36	-0.72	0.32
-2.5	-0.53	0.42	-0.76	0.25

Table 7: Parameters for the Polónyi potential with $\beta = 2 - \sqrt{3}$.

φ_i	$\overline{w}_0$	z_t	w_0	w_1
-1.5	-0.74	0.55	-0.77	0.21
-1.6	-0.69	0.49	-0.76	0.27
-1.7	-0.64	0.43	-0.75	0.32
-1.8	-0.60	0.40	-0.75	0.35
-1.9	-0.56	0.39	-0.76	0.36
-2.0	-0.54	0.38	-0.76	0.36

Table 8: Parameters for the Polónyi potential with $\beta = 0.2$.

φ_i	$\overline{w}_0$	z_t	w_0	w_1
-1.5	-0.73	0.58	-0.68	0.02
-1.6	-0.68	0.49	-0.66	0.07
-1.7	-0.63	0.40	-0.64	0.12
-1.8	-0.58	0.35	-0.63	0.15
-1.9	-0.54	0.32	-0.63	0.17
-2.0	-0.51	0.30	-0.63	0.18

Table 9: Parameters for the Polónyi potential with $\beta = 0.4$.

3.7 SUGRA Potential

The SUGRA potential $e^{\varphi^2/2}/\varphi^\alpha$ is derived from $N = 1$ supergravity [30, 31, 6, 32]. The minimum of the potential occurs at $\varphi = \sqrt{\alpha}$, and $m_\phi^2 = 6H_\Lambda^2$. We will take $\alpha = 4$, which has the interesting property that the minimum of the potential $V_{min} \sim M^8/M_P^4 \sim \rho_\Lambda$ for $M \sim M_{weak} \sim 1$ TeV [6].

φ_i	$\overline{w}_0$	z_t	w_0	w_1
10^{-6}	-0.68	0.50	-0.86	0.35
0.1	-0.68	0.50	-0.86	0.35
0.5	-0.67	0.50	-0.86	0.36
1	-0.74	0.53	-0.82	0.36
1.5	-0.94	0.68	-0.93	0.06
1.9	-0.998	0.67	-0.997	0.001
2.1	-0.998	0.67	-0.997	0.001
2.5	-0.96	0.68	-0.94	0.01
3	-0.85	0.69	-0.79	0.07
3.5	-0.65	0.39	-0.63	0.26
4	-0.44	0.14	-0.57	0.53

Table 10: Parameters for the SUGRA potential.

Results for the SUGRA potential are presented in Figs. 27–30 and Table 10. At present φ is evolving toward the location of the minimum of the potential. For φ_i near the minimum of V at $\varphi = 2$, the SUGRA potential cosmology approaches ΛCDM. For $\varphi_i \geq 4$, $\overline{w}_0$ and w_0 are much too high.

The transition redshift $z_t \approx 0.5$ for $0 < \varphi_i \lesssim 1$. For $0 < \varphi_i \leq 0.5$, asymptotic values $\overline{w}_0 = -0.68$, $z_t = 0.50$, $w_0 = -0.86$, and $w_1 = 0.35$ are obtained, which makes these SUGRA model values robust. These asymptotic values are in excellent agreement with the observed central values. (There is also a very small interval $\varphi_i = 3.3$–3.55 which yields $z_t = 0.33$–0.59.)

4 Conclusion

All seven potentials can closely mimic the ΛCDM model at low redshifts, but only the SUGRA and Polónyi potentials can realize a transition redshift of $z_t \approx 0.5$ for $\Omega_{\Lambda 0} = 0.70$. The other five models predict $z_t \geq 0.67$.

The SN Ia central value $z_t \approx 0.5$ can naturally be explained either by the SUGRA potential with $0 < \varphi_i \lesssim 1$ or by the Polónyi potential with $-2.0 \lesssim \varphi_i \lesssim -1.5$. For just the solutions with $z_t \approx 0.5$, (i) Ω_ϕ becomes significant noticeably earlier than Ω_Λ for ΛCDM and (ii) either w has a maximum near $z = 1$ or w evolves rapidly between $z = 5$ and the present (SUGRA $0 < \varphi_i \leq 0.5$). The SUGRA range of initial values does not involve fine tuning, and has the advantage of also offering a explanation (when $\alpha = 4$) of the parametric relationship $\rho_\Lambda \sim M_{weak}^8/M_P^4$.

The low-z ($0 \leq z \leq 5$) data on z_t, $\overline{w}_0$, w_0, and w_1, although clearly capable of ruling out a cosmological constant, cannot easily distinguish between the stable and unstable de Sitter cases for the cosh potentials, between the two axion potentials, or among the three different Polónyi potential cases. There is no clear distinguishing signal like the sign of w_1. However, knowledge of $w(z)$ for $0 \leq z \leq 5$ does hold out the prospect—if $\Omega_{\Lambda 0}$ is actually due to quintessence—of determining which quintessence potential nature may have chosen.

References

[1] A. G. Riess *et al.* [Supernova Search Team Collaboration], astro-ph/0402512.

[2] R. Kallosh, A. D. Linde, S. Prokushkin, and M. Shmakova, Phys. Rev. D **66**, 123503 (2002), hep-th/0208156.

[3] R. Kallosh, A. D. Linde, S. Prokushkin, and M. Shmakova, Phys. Rev. D **65**, 105016 (2002), hep-th/0110089.

[4] R. Kallosh and A. D. Linde, Phys. Rev. D **67**, 023510 (2003), hep-th/0208157.

[5] M. Tegmark *et al.* [SDSS Collaboration], Phys. Rev. D **69**, 103501 (2004), astro-ph/0310723.

[6] P. Brax, J. Martin, and A. Riazuelo, Phys. Rev. D **64**, 083505 (2001), hep-ph/0104240.

[7] J. S. Alcaniz and N. Pires, astro-ph/0404146.

[8] G. R. Dvali, G. Gabadadze and M. Porrati, Phys. Lett. B **485**, 208 (2000), hep-th/0005016.

[9] C. L. Gardner, Phys. Rev. D **68**, 043513 (2003), astro-ph/0305080.

[10] L. Anchordoqui and H. Goldberg, Phys. Rev. D **68**, 083513 (2003), hep-ph/0306084.

[11] S. J. Gates and B. Zwiebach, Phys. Lett. B **123**, 200 (1983).

[12] C. M. Hull and N. P. Warner, Class. Quant. Grav. **5**, 1517 (1988).

[13] G. W. Gibbons and C. M. Hull, hep-th/0111072.

[14] P. Fré, M. Trigiante, and A. Van Proeyen, Class. Quant. Grav. **19**, 4167 (2002), hep-th/0205119.

[15] R. Kallosh, hep-th/0205315.

[16] C. Wetterich, Nucl. Phys. B **302**, 668 (1988).

[17] P. G. Ferreira and M. Joyce, Phys. Rev. D **58**, 023503 (1998), astro-ph/9711102.

[18] E. J. Copeland, A. R. Liddle, and D. Wands, Phys. Rev. D **57**, 4686 (1998), gr-qc/9711068.

[19] M. Doran and C. Wetterich, Nucl. Phys. Proc. Suppl. **124**, 57 (2003), astro-ph/0205267.

[20] P. K. Townsend, JHEP **0111**, 042 (2001), hep-th/0110072.

[21] L. Andrianopoli, M. Bertolini, A. Ceresole, R. D'Auria, S. Ferrara, P. Fré, and T. Magri, J. Geom. Phys. **23**, 111 (1997), hep-th/9605032.

[22] J. Weller and A. Albrecht, Phys. Rev. D **65**, 103512 (2002), astro-ph/0106079.

[23] U. J. Lopes Franca and R. Rosenfeld, JHEP **0210**, 015 (2002), astro-ph/0206194.

[24] C. M. Hull, Class. Quant. Grav. **2**, 343 (1985).

[25] J. A. Frieman, C. T. Hill, A. Stebbins, and I. Waga, Phys. Rev. Lett. **75**, 2077 (1995), astro-ph/9505060.

[26] I. Waga and J. A. Frieman, Phys. Rev. D **62**, 043521 (2000), astro-ph/0001354.

[27] K. Choi, Phys. Rev. D **62**, 043509 (2000), hep-ph/9902292.

[28] J. Polónyi, Hungary Central Inst Res–KFKI-77-93 (1978).

[29] H. P. Nilles, Phys. Rept. **110**, 1 (1984).

[30] P. Brax and J. Martin, Phys. Lett. B **468**, 40 (1999), astro-ph/9905040.

[31] P. Brax and J. Martin, Phys. Rev. D **61**, 103502 (2000), astro-ph/9912046.

[32] E. J. Copeland, N. J. Nunes, and F. Rosati, Phys. Rev. D **62**, 123503 (2000), hep-ph/0005222.

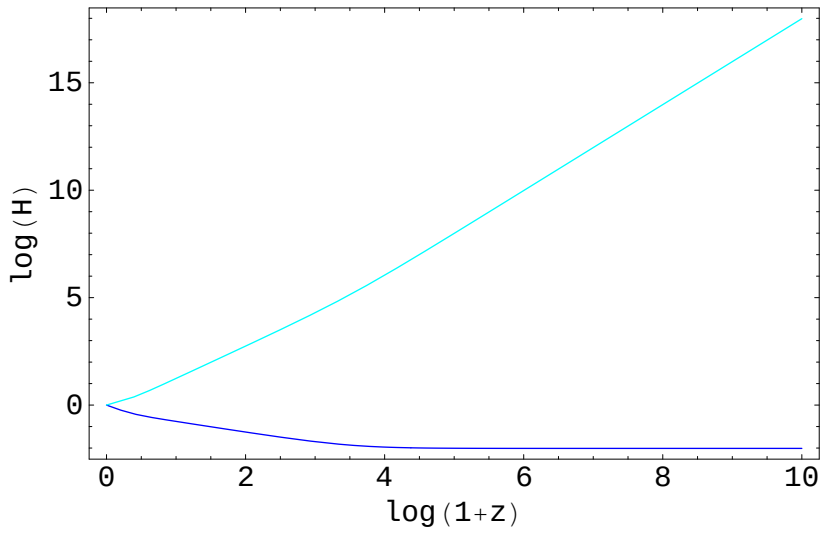

Figure 1: Log_{10} of $\tilde{H}$ (blue, bottom) vs. $\overline{H}$ (cyan, top) for the $e^{\sqrt{2}\varphi}$ potential.

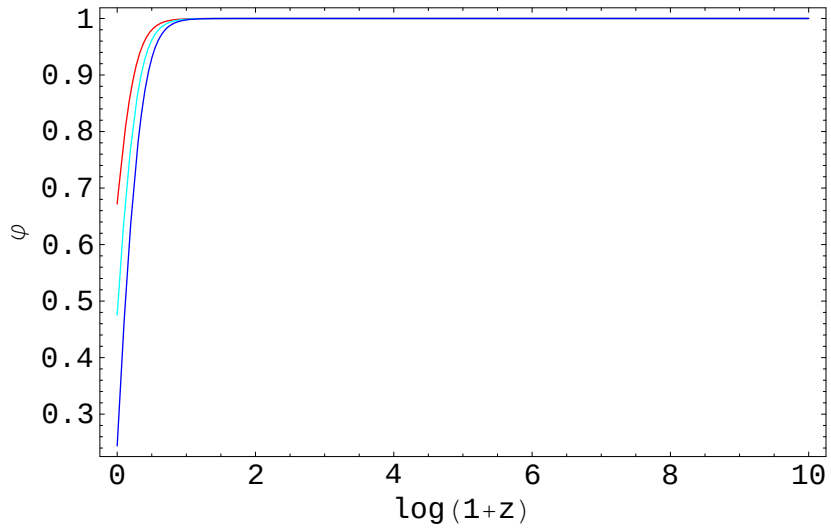

Figure 2: $\varphi(\tau)$ for the exponential potential $e^{\lambda\varphi}$. $\lambda = 1$ (red), $\sqrt{2}$ (cyan), and $\sqrt{3}$ (blue) from top to bottom.

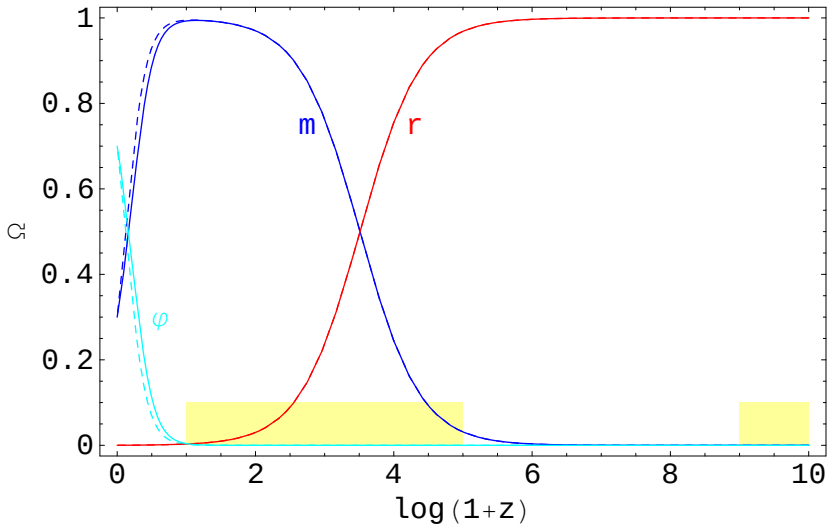

Figure 3: Ω for the exponential potential $e^{\sqrt{2}\varphi}$ (solid) vs. ΛCDM (dotted). The light yellow rectangles are the bounds on Ω_ϕ from LSS, CMB, and BBN.

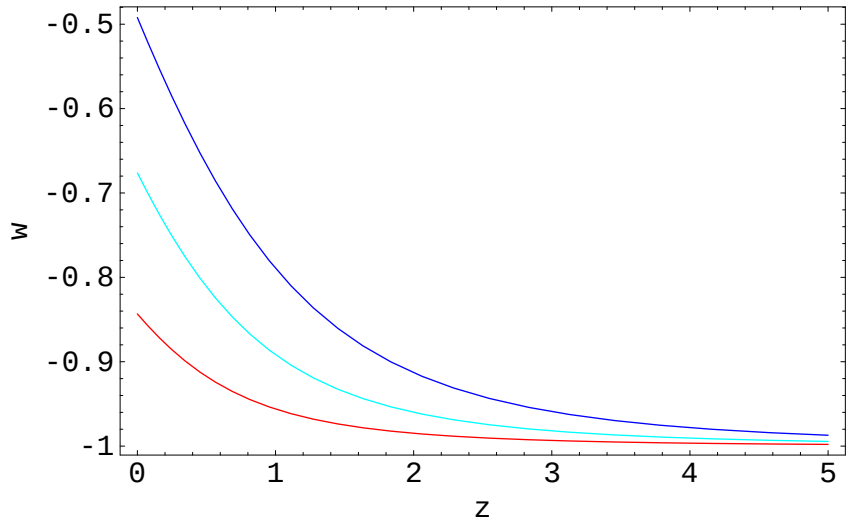

Figure 4: w for the exponential potential $e^{\lambda\varphi}$. $\lambda = 1$ (red), $\sqrt{2}$ (cyan), and $\sqrt{3}$ (blue) from bottom to top.

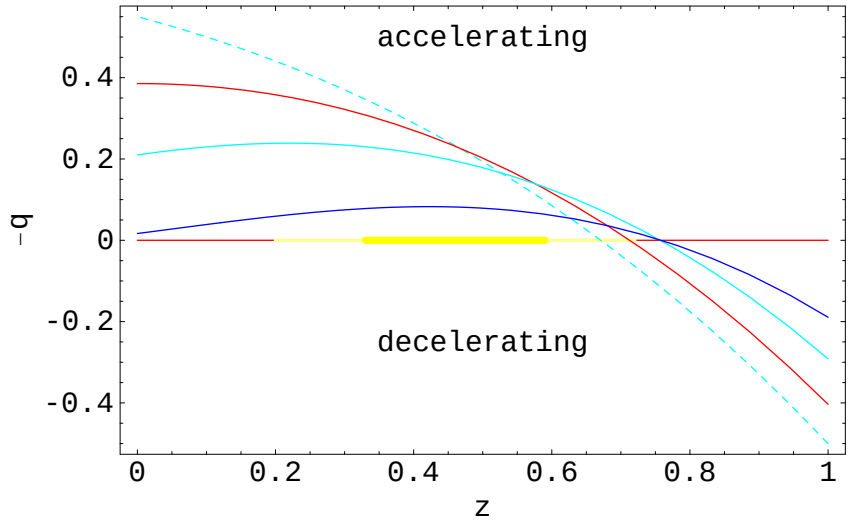

Figure 5: Acceleration parameter $-q$ for the exponential potential $e^{\lambda\varphi}$ (solid) vs. ΛCDM (dotted). The dark and light yellow lines indicate the 1σ and 2σ bounds, respectively, on z_t. $\lambda = 1$ (red), $\sqrt{2}$ (cyan), and $\sqrt{3}$ (blue) from top to bottom at the left.

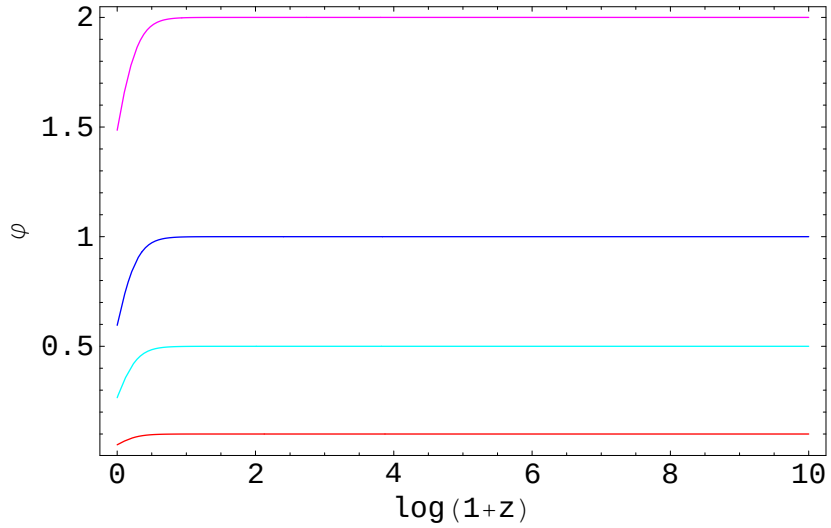

Figure 6: $\varphi(\tau)$ for the potential $\cosh(\sqrt{2}\varphi)$. $\varphi_i = 0.1$ (red), 0.5 (cyan), 1 (blue), and 2 (magenta).

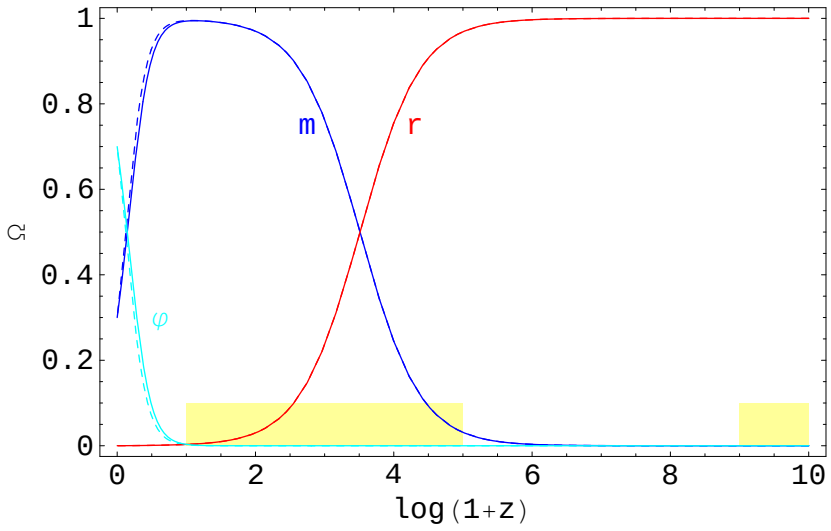

Figure 7: Ω for the potential $\cosh(\sqrt{2}\varphi)$, $\varphi_i = 1$ (solid) vs. ΛCDM (dotted).

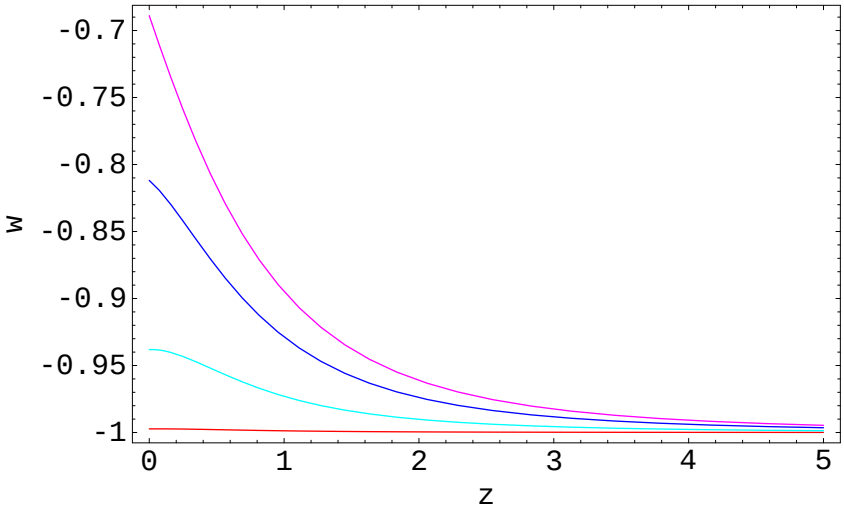

Figure 8: w for the potential $\cosh(\sqrt{2}\varphi)$. $\varphi_i = 0.1$ (red), 0.5 (cyan), 1 (blue), and 2 (magenta) from bottom to top.

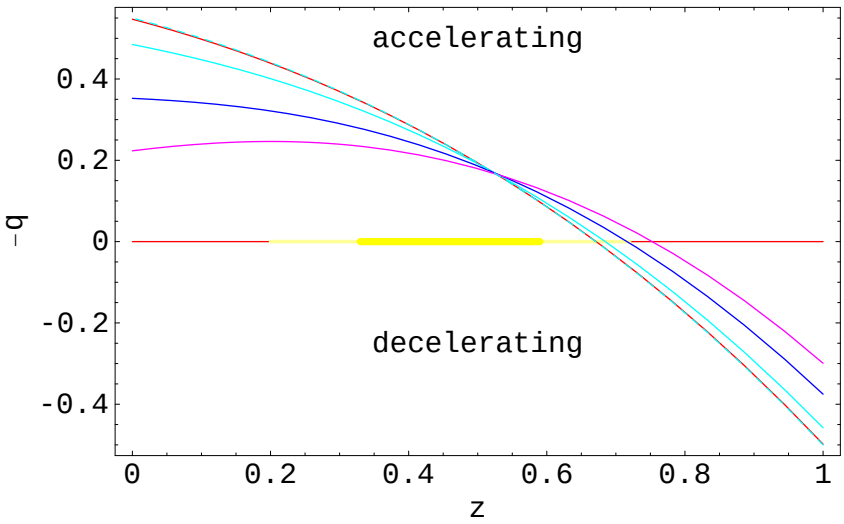

Figure 9: Acceleration parameter $-q$ for the potential $\cosh(\sqrt{2}\varphi)$ (solid) vs. ΛCDM (dotted). $\varphi_i = 0.1$ (red), 0.5 (cyan), 1 (blue), and 2 (magenta) from top to bottom at the left.

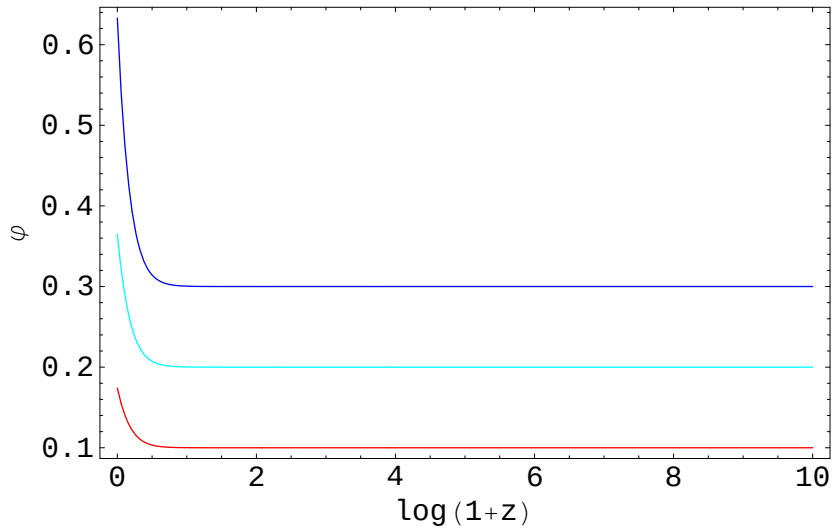

Figure 10: $\varphi(\tau)$ for the potential $2 - \cosh(\sqrt{2}\varphi)$. $\varphi_i = 0.1$ (red), 0.2 (cyan), and 0.3 (blue).

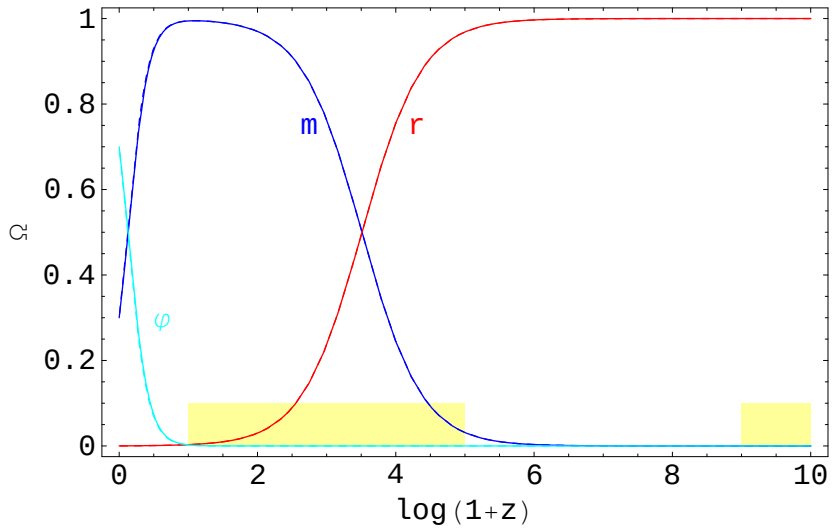

Figure 11: Ω for the potential $2 - \cosh(\sqrt{2}\varphi)$, $\varphi_i = 0.2$ (solid) vs. ΛCDM (dotted).

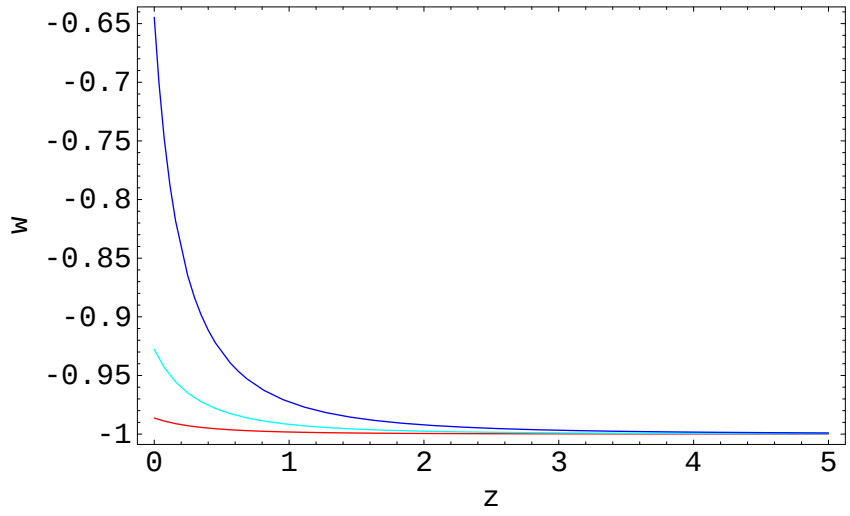

Figure 12: w for the potential $2 - \cosh(\sqrt{2}\varphi)$. $\varphi_i = 0.1$ (red), 0.2 (cyan), and 0.3 (blue) from bottom to top.

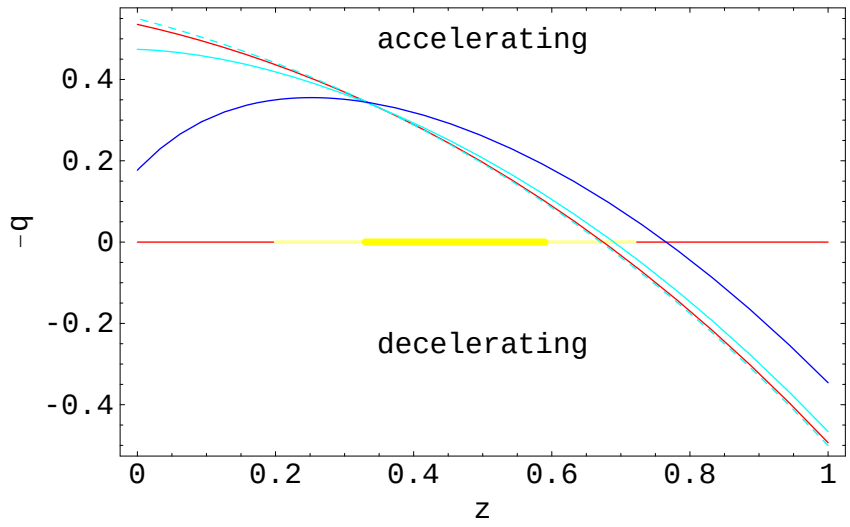

Figure 13: Acceleration parameter $-q$ for the potential $2-\cosh(\sqrt{2}\varphi)$ (solid) vs. ΛCDM (dotted). $\varphi_i = 0.1$ (red), 0.2 (cyan), and 0.3 (blue) from top to bottom at the left.

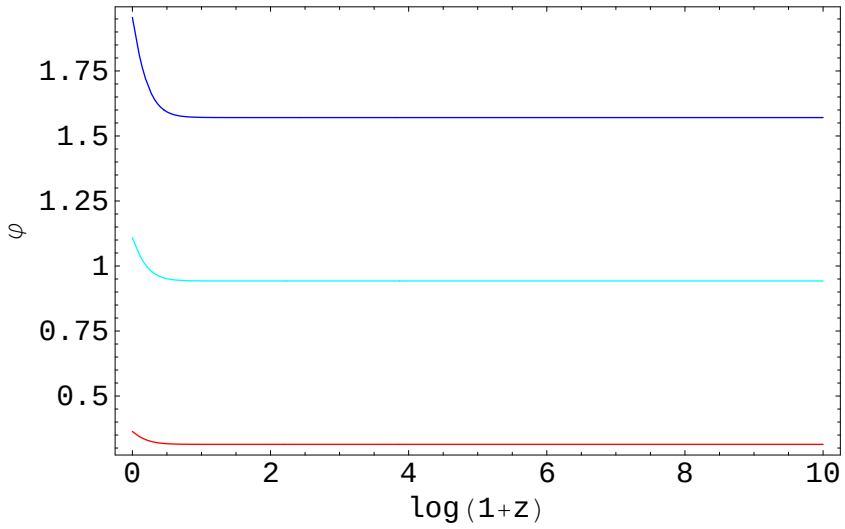

Figure 14: $\varphi(\tau)$ for the potential $1 + \cos(\varphi)$. $\varphi_i/\pi = 0.1$ (red), 0.3 (cyan), and 0.5 (blue).

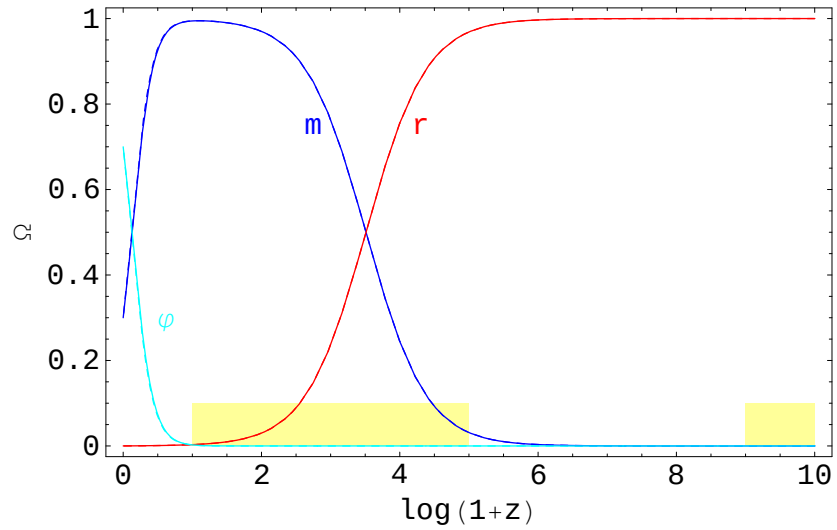

Figure 15: Ω for the potential $1 + \cos(\varphi)$, $\varphi_i/\pi = 0.3$ (solid) vs. ΛCDM (dotted).

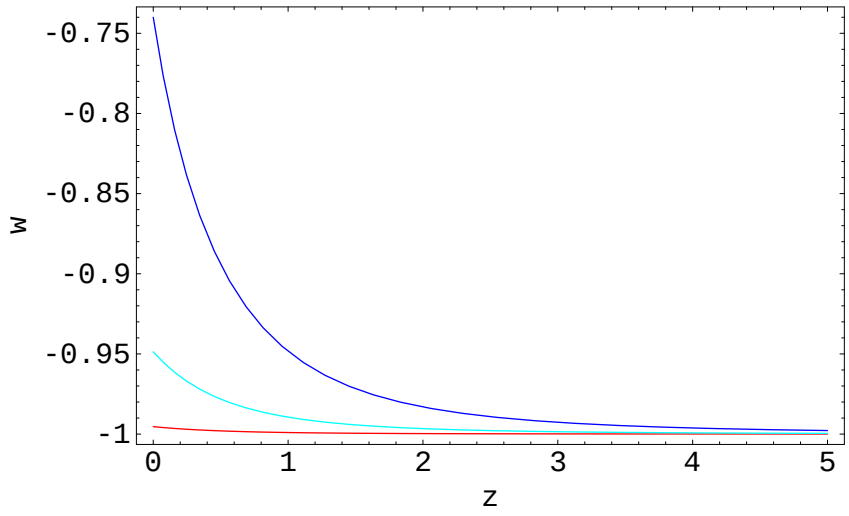

Figure 16: w for the potential $1+\cos(\varphi)$. $\varphi_i/\pi = 0.1$ (red), 0.3 (cyan), and 0.5 (blue) from bottom to top.

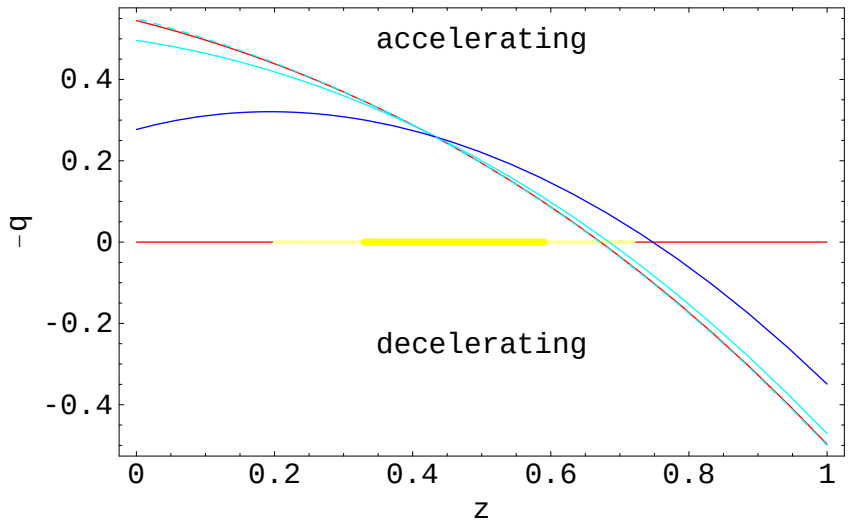

Figure 17: Acceleration parameter $-q$ for the potential $1+\cos(\varphi)$ (solid) vs. ΛCDM (dotted). $\varphi_i/\pi = 0.1$ (red), 0.3 (cyan), and 0.5 (blue) from top to bottom at the left.

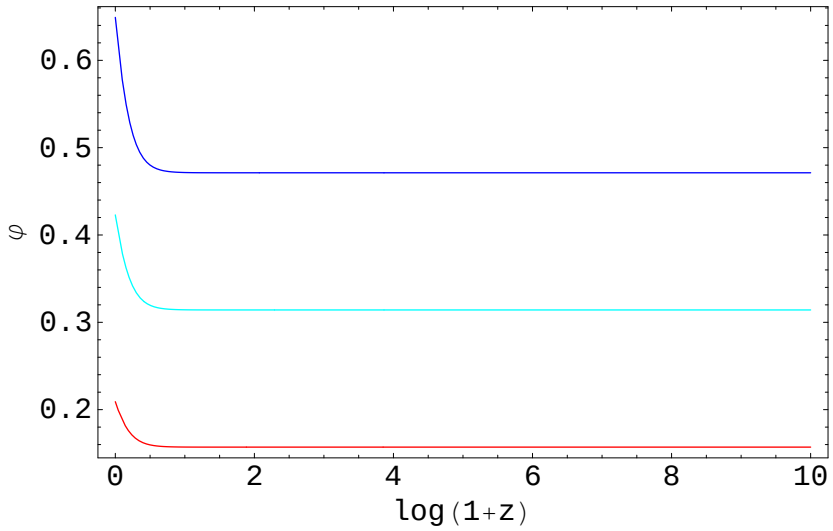

Figure 18: $\varphi(\tau)$ for the potential $\cos(\varphi)$. $\varphi_i/\pi = 0.05$ (red), 0.1 (cyan), and 0.15 (blue).

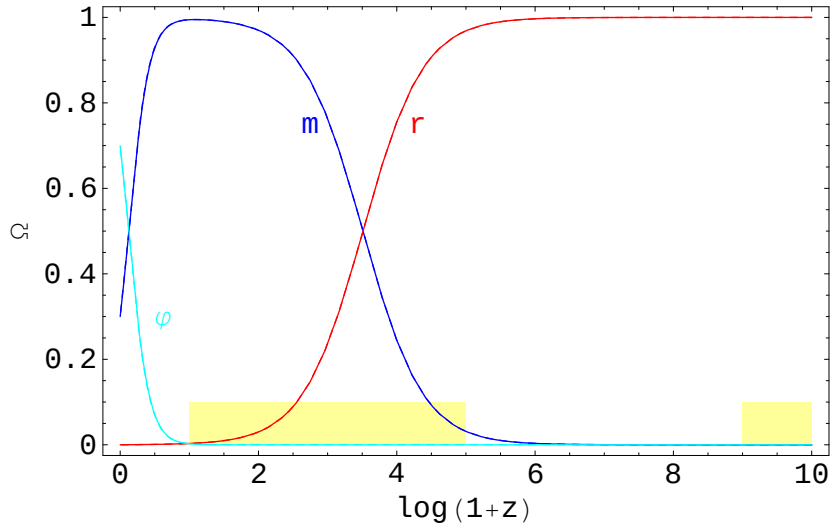

Figure 19: Ω for the potential $\cos(\varphi)$, $\varphi_i/\pi = 0.1$ (solid) vs. ΛCDM (dotted).

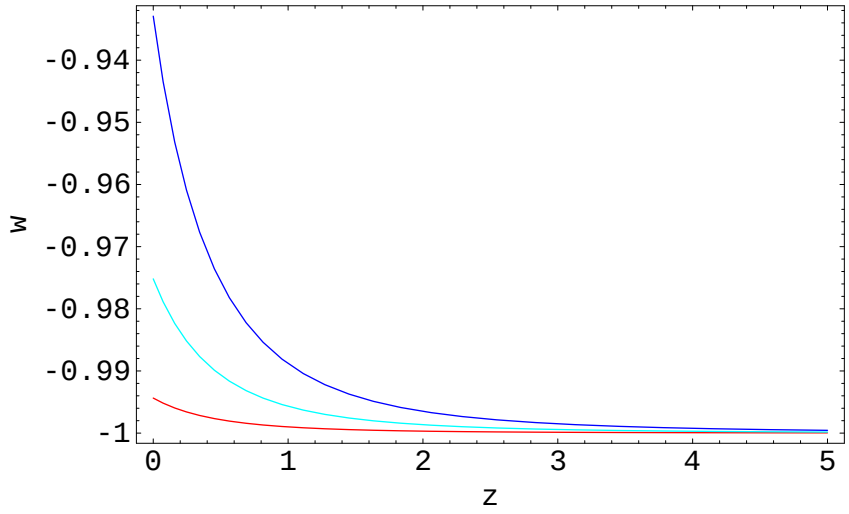

Figure 20: w for the potential $\cos(\varphi)$. $\varphi_i/\pi = 0.05$ (red), 0.1 (cyan), and 0.15 (blue) from bottom to top.

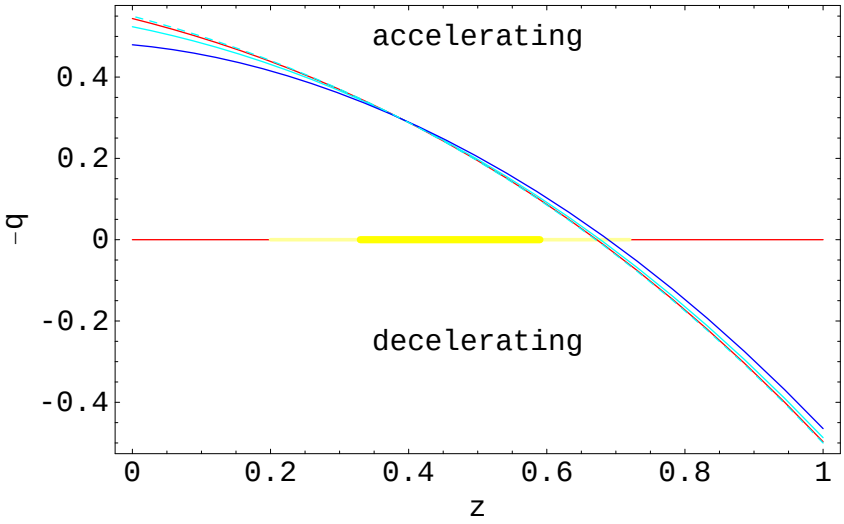

Figure 21: Acceleration parameter $-q$ for the potential $\cos(\varphi)$ (solid) vs. ΛCDM (dotted). $\varphi_i/\pi = 0.05$ (red), 0.1 (cyan), and 0.15 (blue) from top to bottom at the left.

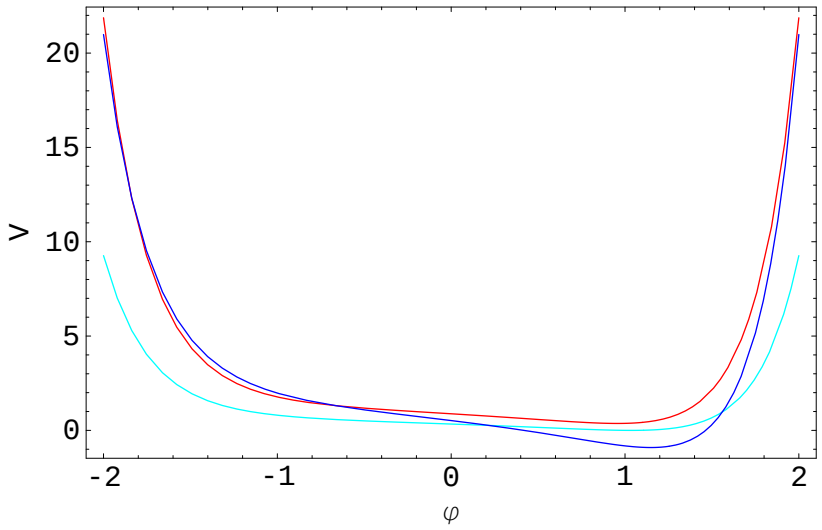

Figure 22: Dimensionless Polónyi potential for $\beta = 2 - \sqrt{3}$ (cyan, $V_{min} = 0$), 0.2 (red, $V_{min} > 0$), and 0.4 (blue, $V_{min} < 0$).

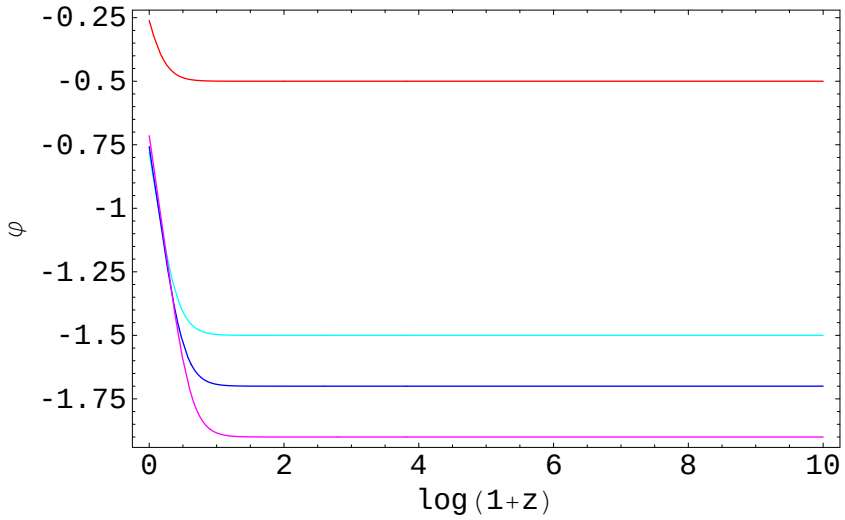

Figure 23: $\varphi(\tau)$ for the Polónyi potential. $\varphi_i = -0.5$ (red), -1.5 (cyan), -1.7 (blue), and -1.9 (magenta).

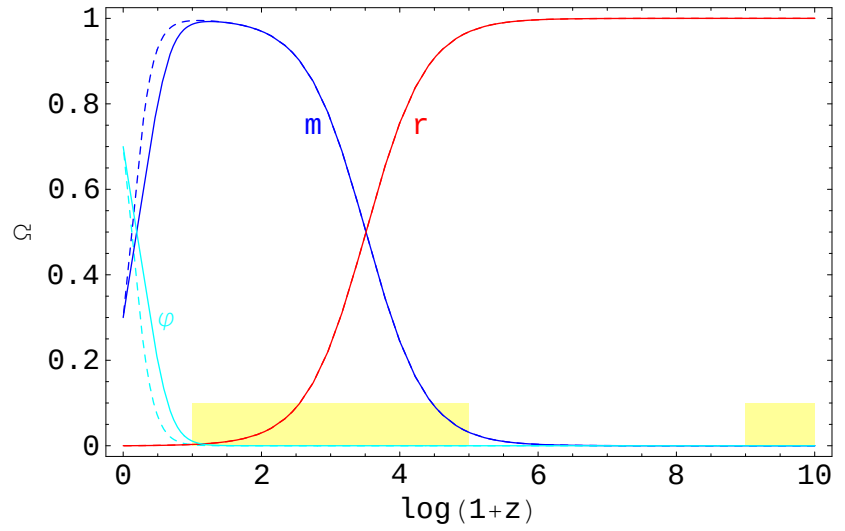

Figure 24: Ω for the Polónyi potential. $\varphi_i = -1.7$ (solid) vs. ΛCDM (dotted).

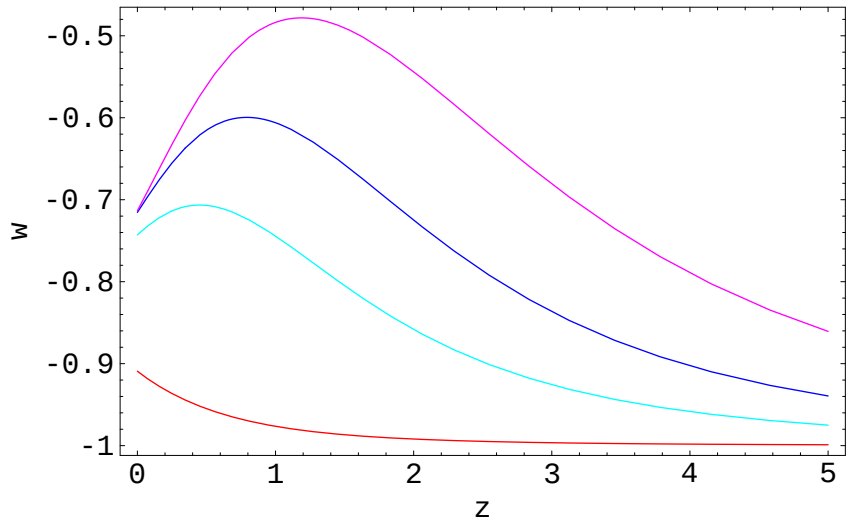

Figure 25: w for the Polónyi potential. $\varphi_i = -0.5$ (red), -1.5 (cyan), -1.7 (blue), and -1.9 (magenta) from bottom to top.

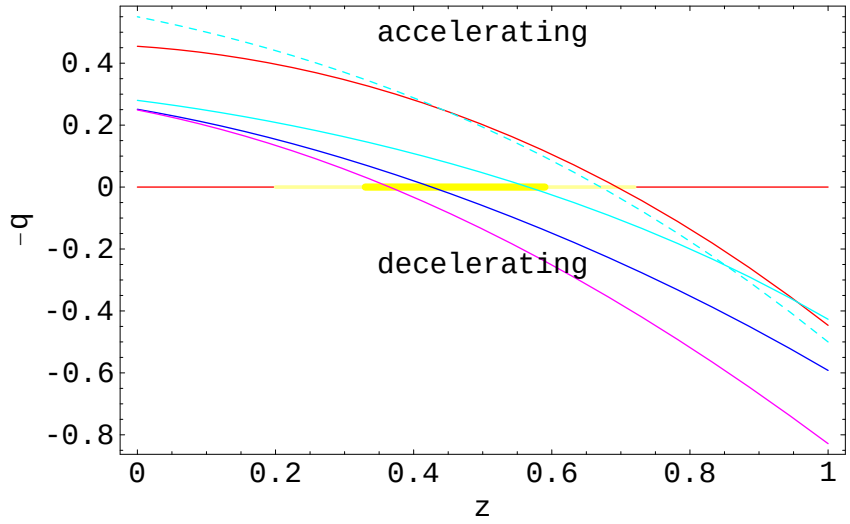

Figure 26: Acceleration parameter $-q$ for the Polónyi potential (solid) vs. ΛCDM (dotted). $\varphi_i = -0.5$ (red), -1.5 (cyan), -1.7 (blue), and -1.9 (magenta) from top to bottom at the left.

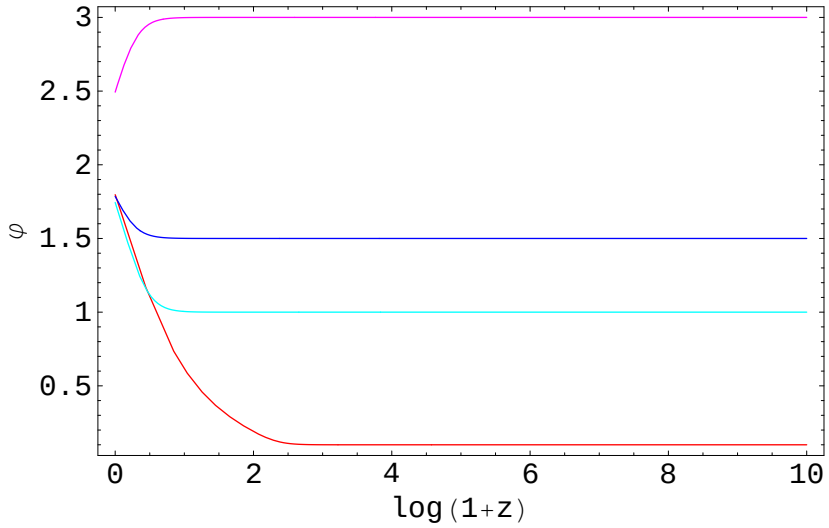

Figure 27: $\varphi(\tau)$ for the SUGRA potential. $\varphi_i = 0.1$ (red), 1 (cyan), 1.5 (blue), and 3 (magenta).

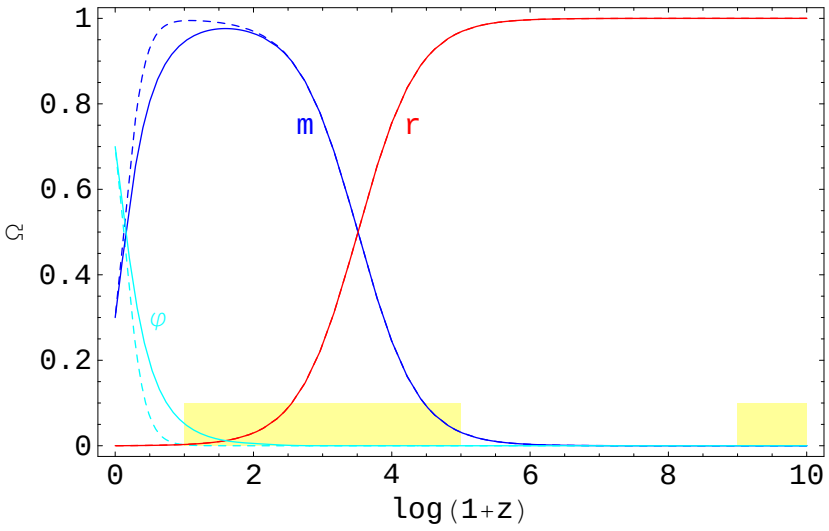

Figure 28: Ω for the SUGRA potential. $\varphi_i = 0.1$ (solid) vs. ΛCDM (dotted).

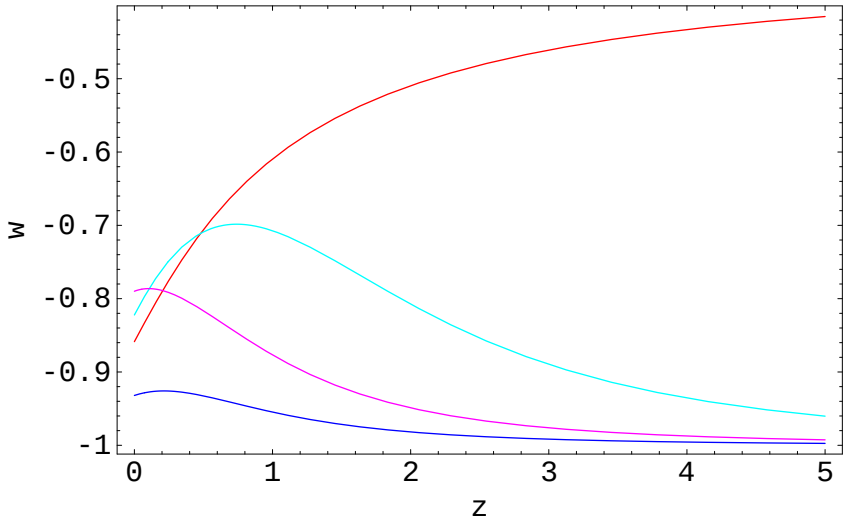

Figure 29: w for the SUGRA potential. $\varphi_i = 0.1$ (red, top), 1 (cyan, second from top), 1.5 (blue, bottom), and 3 (magenta, third from top) at the right.

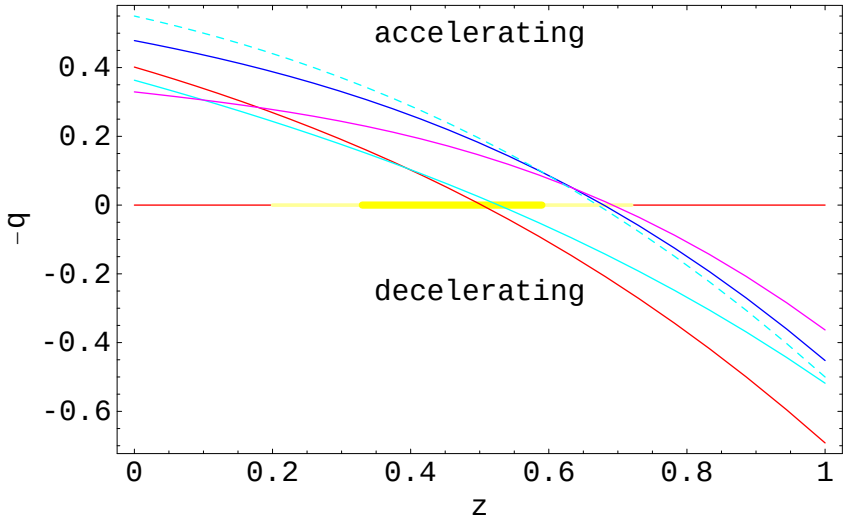

Figure 30: Acceleration parameter $-q$ for the SUGRA potential (solid) vs. ΛCDM (dotted). $\varphi_i = 0.1$ (red), 1 (cyan), 1.5 (blue), and 3 (magenta) from bottom to top at the right.